Research Square

Preprints are preliminary reports that have not undergone peer review.
They should not be considered conclusive, used to inform clinical practice,
or referenced by the media as validated information.

Bcl-2 suppresses ER-mitochondrial Ca2+ transfer by directly limiting ER-mitochondrial contact sites

Geert Bultynck

geert.bultynck@kuleuven.be

KU Leuven https://orcid.org/0000-0002-5968-4828

Manon Callens

KU Leuven

Jens Loncke

KU Leuven

Dmitry Lim

Università degli Studi del Piemonte Orientale https://orcid.org/0000-0002-4316-2654

Rita La Rovere

Ophélie Champion

Centre de Recherche en Cancérologie et Immunologie intégrée Nantes Angers, INSERM, CNRS
https://orcid.org/0009-0003-1329-6306

Tim Vervliet

KU Leuven https://orcid.org/0000-0002-4030-5875

Article

Keywords: Anti-apoptotic Bcl-2, ER-mitochondrial contact sites, SPLICS, mitochondrial Calcium dynamics, IP3 receptor

Posted Date: August 13th, 2026

DOI: https://doi.org/10.21203/rs.3.rs-10449449/v1

License: This work is licensed under a Creative Commons Attribution 4.0 International License.
Read Full License

Additional Declarations: (Not answered)

Bcl-2 suppresses ER-mitochondrial Ca^{2+} transfer by directly limiting ER-mitochondrial contact sites

Manon Callens[1], Jens Loncke[1], Ophélie Champion[1], Dmitry Lim[2], Rita La Rovere[1], Tim Vervliet[1], Geert Bultynck[1]

[1] KU Leuven, Laboratory of Molecular & Cellular Signaling, Department of Cellular and Molecular Medicine, Campus Gasthuisberg O/N-1 bus 802, Herestraat 49, BE-3000 Leuven, Belgium

[2] Università del Piemonte Orientale, Department of Pharmaceutical Sciences, 28100, Novara, Italy

Keywords

Anti-apoptotic Bcl-2; ER-mitochondrial contact sites; SPLICS; mitochondrial Calcium dynamics; IP_3 receptor

Abbreviations

AD	Alzheimer's disease
Bcl-2	B-cell lymphoma 2
DLBL	Diffuse large B-cell lymphoma
DMSO	Dimethylsulfoxide
EML	ER-mitochondrial linkers
GRP75	Glucose-related protein 75
IP_3R	Inositol 1,4,5-trisphosphate receptor
MERCS	Mitochondria-endoplasmic reticulum contact sites
Mfn2	Mitofusin 2
MOMP	Mitochondrial outer membrane permeabilization
OCR	Oxygen consumption rate
OXPHOS	Oxidative phosphorylation
PARP	Poly (ADP-ribose) polymerase
RyR	Ryanodine receptor
STS	Staurosporine
VAPB	Vesicle-associated membrane protein-associated protein B/C
VDAC1	Voltage-dependent anion channel 1

Abstract

Anti-apoptotic B cell lymphoma (Bcl-2) tightly regulates apoptosis by controlling mitochondrial outer membrane permeabilization and intracellular Ca^{2+} dynamics. At the endoplasmic reticulum (ER), Bcl-2 directly inhibits inositol 1,4,5-trisphosphate receptors (IP_3Rs), intracellular Ca^{2+}-release channels, thereby limiting mitochondrial Ca^{2+} overload. Yet, Bcl-2's non-canonical function in cells not exposed to apoptotic insults remains poorly understood. Here, we set out to study this function by generating CRISPR-Cas9-mediated Bcl-2 knockout (Bcl-2 KO) in HeLa cells, which are not dependent on Bcl-2 for their survival. Bcl-2 KO did not evoke spontaneous cell death, but enhanced mitochondrial respiration. Mechanistically, Bcl-2 KO increased mitochondrial Ca^{2+} uptake, which was restored by Bcl-2 re-expression. Moreover, Bcl-2-deficient cells displayed increased mitochondria-ER contact sites (MERCS), including short contacts (10 nm) and contacts at an optimal distance (20 nm) for efficient ER-mitochondrial Ca^{2+} transfer, without altering the abundance of major MERCS-tethering proteins. Enforcing a 20 nm ER-mitochondrial distance using 20 nm molecular rulers increased mitochondrial Ca^{2+} influx in control cells to similar levels as those in Bcl-2 KO cells. *Vice versa*, Bcl-2 overexpression limited the number of 10 and 20 nm MERCS, an effect of Bcl-2 that was largely dependent on the presence of IP_3Rs. Therefore, we identified a novel role of Bcl-2 at MERCS where it controls ER-mitochondrial distance, thereby providing a yet unappreciated action of Bcl-2 that helps preventing mitochondrial Ca^{2+} overload. These new insights into Bcl-2's non-canonical role may contribute to a better understanding of altered ER-mitochondrial Ca^{2+} signalling in disease conditions associated with Bcl-2 upregulation such as haematological cancers.

Introduction

The B-cell lymphoma-2 (Bcl-2) protein is a central regulator of cellular homeostasis, best known for its anti-apoptotic functions. As the founding member of the Bcl-2-protein family, Bcl-2 functions within a tightly regulated network of pro- and anti-apoptotic proteins that collectively determine mitochondrial outer membrane permeabilization (MOMP), the onset of apoptotic cell death [1,2].

The Bcl-2-protein family consists of pro-apoptotic and anti-apoptotic members, classified based on their function and the presence of Bcl-2 homology (BH) domains. Upon activation, the pro-apoptotic members BAX/BAK oligomerize and form protein-permeable pores that execute MOMP, leading to the release of cytochrome c and SMAC/Diablo from the intermembrane space with subsequent activation of downstream apoptotic signalling. The activity of BAX/BAK is tightly regulated by two opposing groups: anti-apoptotic proteins, including Bcl-2, which sequester and inhibit pro-apoptotic proteins, and BH3-only proteins, which either directly activate BAX/BAK (such as Bim and tBid) or act as sensitizers by binding to and antagonizing anti-apoptotic Bcl-2-family members (such as Bad) [3].

Bcl-2 proteins are well known for their role in cancers, particularly in haematological malignancies [4]. Due to oncogenic stress, such cancer cells upregulate pro-apoptotic BH3-only proteins, such as Bim, that require concomitant upregulation of Bcl-2, thereby neutralizing Bim and enabling cancer cell survival. Therefore, these cancer cells become highly dependent on Bcl-2 for their survival, making pharmacological inhibition of Bcl-2 an attractive anticancer strategy with limited toxicity towards normal, healthy cells [4-6]. The BH3-mimetic venetoclax is a selective Bcl-2 antagonist and is used in the clinic to treat patients with chronic lymphocytic leukemia and acute myeloid leukemia [7,8]. Nowadays, next-generation BH3 mimetics such as sonrotoclax have been developed to overcome acquired venetoclax resistance caused by Bcl-2 mutations, which has recently received FDA approval for the treatment of relapsed or refractory mantle cell lymphoma[9,10].

Beyond their role in regulating cell death and survival, anti-apoptotic Bcl-2-family members have also been implicated in non-canonical functions, including modulation of intracellular Ca^{2+} dynamics and mitochondrial bioenergetics [11,12]. Bcl-2 localizes to the endoplasmic reticulum (ER) and mitochondria [13], key organelles mediating Ca^{2+} storage and signalling. Bcl-2, in particular via its BH4 domain, interacts with and inhibits inositol 1,4,5-trisphosphate receptors (IP_3Rs) and ryanodine receptors (RyRs), which are the main Ca^{2+} release channels located in the ER [11,14,15]. By inhibiting IP_3Rs, Bcl-2 suppresses ER-derived Ca^{2+} fluxes, thereby also suppressing Ca^{2+} accumulation in mitochondria [16]. Importantly, ER-mitochondrial Ca^{2+} transfers occur via mitochondria-endoplasmic reticulum contact sites (MERCS)[17], particularly those of about 20 nm distance between ER and mitochondria [18]. MERCS are regions where the ER and the mitochondrial membrane reside in close

contact, linking Ca^{2+}-transport systems from the ER, namely IP_3Rs, with those from the mitochondrial outer membrane, namely voltage-dependent anion channels type 1 (VDAC1) via the chaperone GRP75 or other mechanisms [19,20]. Moreover, the Ca^{2+}-signalling hotspots/nanodomains established by MERCS play a critical role in controlling cell function contributing to cell survival on the one hand by sustaining mitochondrial metabolism in response to Ca^{2+} oscillations, and cell death on the other hand by mitochondrial Ca^{2+} overload in response to persistent, excessive [Ca^{2+}] elevations [21,22]. Fascinatingly, in several cell types/models including mouse embryonic fibroblasts and HeLa cells, Bcl-2 has been found to also reside at MERCS [13,23]. Moreover, Bcl-2 is present in virtually all cells, yet it's daily function in cells not exposed to apoptotic triggers remains poorly understood. Given the importance of MERCS for cell function, we set out to determine the function of endogenous Bcl-2 at MERCS by generating Bcl-2-knockout HeLa cells. Our choice for HeLa cells was motivated by three factors: (i) HeLa cells are not dependent on endogenous Bcl-2 for their survival ([24] and this study) thus avoiding secondary effects due to cell death confounding our findings when knocking out Bcl-2, (ii) HeLa cells are known to display efficient coupling between ER and mitochondria with between 5 to 20 % of the mitochondrial surface coupled to the ER [25,26], (iii) despite having low Bcl-2-protein levels, Bcl-2 can be detected in mitochondria-associated ER membrane (MAMs), which are biochemical isolated membrane fractions of MERCS [27]. Our work revealed a non-canonical role for endogenous Bcl-2 directly limiting short (10 nm) and medium (20 nm) "Ca^{2+}" MERCS, thereby efficiently preventing mitochondrial Ca^{2+} overload. Mechanistically, Bcl-2's function at MERCS is dependent on the presence of IP_3Rs, severing as hubs for Bcl-2 at MERCS.

Material and Methods

Reagents and Antibodies

All reagents were obtained from Thermo Fisher Scientific (Merelbeke, Belgium) unless stated otherwise.

The following antibodies were used: mouse monoclonal anti-Bcl-2 (1 :500, Santa Cruz, sc-7382), mouse monoclonal anti-vinculin (1:10000, Merck, V9131), rabbit monoclonal anti-PARP (1:1000, Cell Signalling, 9532S), rabbit monoclonal BCL-XL (1:1000, Thermo scientific, MA5-15142), rabbit polyclonal anti-MCL-1 (1:500, Cell Signalling Technology, 4572), mouse monoclonal anti-GAPDH (1:10.000, Sigma-Aldrich G8795), rabbit polyclonal anti-IP_3R (1:1000, Rbt475, inhouse-made [28]), rabbit polyclonal anti-VDAC1 (1:1000, Cell Signalling Technology, 4866)

Cell culture

HeLa cells were cultured at 37°C in the presence of 5% CO2 in Dulbecco's Modified Eagle Medium (DMEM) (Gibco) supplemented with 10% foetal calf serum (Serana), 1% non-essential amino acids (Gibco), 4 mM L-glutamine, (Gibco) 100 units/ml penicillin (Gibco) and 100 µg/ml streptomycin (Gibco). OCI-LY-1 and SU-DHL-4 diffuse large B-cell lymphoma (DLBCL) cell lines were kindly gifted by Dr. Anthony Letai (Dana-Farber Cancer Institute, Boston, Massachusetts, USA). OCI-LY-1 cells were cultured in suspension in Iscove modified Dulbecco's medium (IMDM, Life Technologies, Brussels, Belgium), supplemented with 20% foetal calf serum (Serana), 4 mM L-glutamine, (Gibco) 100 units/ml penicillin (Gibco) and 100 µg/ml streptomycin (Gibco). SU-DHL-4 cells were cultured in suspension in Roswell Park Memorial Institute (RPMI-1640) medium (Life Technologies, Brussels, Belgium) supplemented with 10% foetal calf serum (Serana), 4 mM L-glutamine, (Gibco) 100 units/ml penicillin (Gibco) and 100 µg/ml streptomycin (Gibco). HeLa triple IP_3R-knockout cells (HeLa IP_3R 3KO cells) were a kind gift from Dr. Mikoshiba [29]. All work with human cell lines was approved by Ethical Committee UZ Leuven (S63808).

All cells were cultured at 37°C in the presence of 5% CO2, in mycoplasma-free conditions which was routinely checked.

Generation of Bcl-2 KO in HeLa cells

HeLa cells were seeded in a 6-well plate and grown until 60-80% confluency. The cells were transfected with 5 µg of pSpCas9(BB)-2A-Puro vector vector containing a guideRNA for Bcl-2 (Bcl-2 KO) or an empty control vector (Cas9 control cells). TransIT-X2® Dynamic Delivery System (Mirus) transfection reagent was used according to the manufacturer's instructions. pSpCas9(BB)-2A-Puro (PX459) was a gift from

Feng Zhang (Addgene plasmid #48139; http://n2t.net/addgene:48139; RRID:Addgene_48139). Transfected cells were selected by adding 2 µg/mL puromycin (InvivoGen) to the culture medium for 48h generating a pool of Bcl-2 knock-out and Cas9 control cells. Knockout of Bcl-2 was verified via immunoblotting. Guide RNA sequence of Bcl-2 was previously described and validated in [30]. After generation of Bcl-2 KO cells, the cells were kept in culture for a maximum of 10 passages. Following 10 passage, a new Bcl-2 KO pool and Cas9 control pool was generated starting again from the original HeLa cells.

Plasmids and constructs

pCMV24-p2a-mCherry and pCMV24-3xFLAG-Bcl-2-p2a-mCherry constructs were created as described in [14]. pCMV G-CEPIA-3mt was kindly gifted by Masamitsu Iino [31] (Addgene plasmid #58219; https://www.addgene.org/58219; RRID:Addgene_58219); pCMV R-CEPIA-1ER was kindly gifted by Masamitsu Iino [31] (Addgene plasmid # 58216; https://www.addgene.org/58216 ;RRID:Addgene 58216).

Generation of pcDNA3.1-ER-mRFP (Addgene plasmid #231176; https://www.addgene.org/231176/; RRID: Addgene 231176), pcDNA3.1-20nmEML-mRFP (Addgene plasmid #231175; https://www.addgene.org/231178/; RRID:Addgene 231178) plasmids has been described elsewhere [18].

Transient transfection

Cells were seeded in four-chamber 35-mm dishes and grown to approximately 60% confluency. TransIT-X2® Dynamic Delivery System (Mirus) transfection reagent was used according to the manufacturer's instructions and medium was refreshed 6h post-transfection. Cells were used for experiments 24h post-transfection.

For experiments with pCMV24-p2a-mCherry or pCMV24-3xFLAG-Bcl-2-p2a-mCherry plasmids, 480ng DNA was used per four-chamber 35-mm dish. For experiments with pCMV G-CEPIA-3mt and pCMV R-CEPIA-1ER, 0.5µg DNA each was used per four-chamber 35-mm dish. For experiments with pcDNA3.1-20nmEML-mRFP or pcDNA3.1-ER-mRFP, 0.5µg DNA was used per four-chamber 35-mm dish.

Immunoblotting

Cells were harvested and lysed in a CHAPS based lysis buffer (50 mM Tris-HCl pH 7.5, 100 mM NaCl, 2 mM EDTA, 1% CHAPS, 50 mM NaF, 1mM Na3VO4 and Pierce protease inhibitor cocktail (Merck, Hoeilaart, Belgium)) for 30 minutes at 4°C. The lysate was centrifuged at 4000 x g and the supernatant

was collected. Protein samples were prepared in NuPAGE LDS Sample buffer (NP0007, Thermo Fisher Scientific) and boiled for 5 min at 95 °C.

Protein samples were separated on a 4-12% Bis/Tris SDS polyacrylamide gel (Invitrogen, Merelbeke, Belgium), transferred to PVDF membranes (Thermo Scientific, Rockford, IL, USA) and blocked with tris-buffered saline containing 0.1% Tween-20 and 5% non-fat dry milk powder. Membranes were incubated with primary antibodies overnight at 4 °C. After 3 wash steps with tris-buffered saline containing 0.1% Tween-20, membranes were incubated for 1 h with secondary antibodies conjugated to horse radish peroxidase. Proteins were visualized by using Pierce® ECL Western Blotting Substrate (Thermo Scientific, Rockford, IL, USA). Images were acquired using the ChemiDoc™ MP System (Bio-Rad, Nazareth, Belgium). Quantification of the images was performed using Image Lab 5.2 software.

Apoptosis assays

Staurosporin experiments: Cells were seeded in 6-well plate and treated with 0.1µM of staurosporine or an equal volume of dimethylsulfoxide (DMSO, Sigma-Aldrich, Overijse, Belgium) for 6 hours. Afterwards, the cells were harvested and lysed with CHAPS buffer, which were analysed via NUPAGE Bis-Tris 3-12% gels and immunoblotting for PARP, quantifying the ratio of cleaved over total PARP * 100 as a %.

Venetoclax experiments: OCI-LY-1 and HeLa cells were incubated for 6h with Venetoclax (Ven) 1µM and vehicle (DMSO) condition was included as a control. Cell death was assessed using Annexin V-FITC/7-AAD staining. Cell death by apoptosis was scored by quantifying the population of Annexin V-FITC-positive cells. Fluorescence acquisition and analysis were performed using an AccuriC6 Plus (BD Biosciences) and FlowJo software.

Single-cell Ca^{2+} measurements

Cells were seeded in seeded in 4 chamber slides with coverslips (IBL, Gerasdorf bei Wien, Austria). Cells were transfected with R-CEPIA-1ER and G-CEPIA-3mt according to transfection protocol or loaded with 1µM Fura-2-AM (Biotium, 50033-1) in modified Krebs buffer (135 mM NaCl, 6.2 mM KCl, 1.2 mM $MgCl_2$, 12 mM HEPES, pH 7.3, 11.5 mM glucose and 2 mM $CaCl_2$) for 30 minutes at room temperature. Subsequently, cells were washed twice in modified Krebs buffer and were allowed to de-esterify for 30 minutes at room temperature. Ca^{2+} imaging was performed using Nikon Eclipse Ti2 inverted microscope with a 20X air or 40X oil objective and PCO edge 4.2 bi CMOS camera. 3 mM EGTA (Sigma-Aldrich) was used to chelate extracellular Ca^{2+} and ATP (1µM or 10µM) was used as agonist. Data was quantified using custom ImageJ scripts and Python scripts, which can be found on: https://github.com/jensloncke .

Confocal imaging of SPLICS probes

ER-mitochondrial contact sites were detected using the SPLICS Mt-ER Short P2A probe (8-10nm, $SPLICS_{short}$), which was kindly gifted by Marisa Brini & Tito Calì (Addgene plasmid #164108 ; http://n2t.net/addgene:164108 ; RRID:Addgene_164108). Generation of SPLICS-20nm-GFPb1-10_pcDNA3.1(+) ($SPLICS_{medium}$) was reported elsewhere [18]. Cells were seeded in 12-well plates on coverslips (Paul Marienfeld, Germany, 0117580) and transfected with the SPLICS probe. 24h post transfection, the cells were fixed with 4% paraformaldehyde. Coverslips were washed with phosphate-buffered saline (PBS) and mounted on glass slides using ProLong Glass Antifade mountant (Invitrogen). Images were acquired on a Nikon TiE A1R confocal microscope equipped with a 60X oil objective. Z-stacks with a depth of 3 µm were acquired and processed using a homemade ImageJ macro, which was made publicly available on Tito Calì's GitHub repository: https://github.com/titocali1/Quantification-Plugins

Seahorse mitochondrial stress test

Cells were plated in an XFp Extracellular Flux Analyzer culture plate in culture medium overnight. Before the assay, cells were switched to MitoStress Test assay medium (Seahorse Biosciences, North Billerica, MA, USA) containing 25 mM Glucose, supplemented with 2 mM Glutamine and 1 mM sodium pyruvate. Oxygen consumption rate (OCR) was measured using the Agilent XFp Extracellular Flux Analyzer (Seahorse Biosciences) according to manufacturer's instructions, with sequential additions of oligomycin (8µM final concentration), FCCP (4.5µM final concentration) and antimycin A (5µM final concentration).

Statistics

Statistical tests were performed using Prism 11 (GraphPad, La Jolla, CA, USA). Data are represented as the mean ± S.D. Assumption of normal distribution was checked via Shapiro-Wilk testing, assumption of equality of variances was tested using Bartlett's test. When both assumptions were fulfilled, student's t-test or one-way *ANOVA with Dunnett's test were performed. When assumptions were not fulfilled, a non-parametric Kruskal-Wallis test or Brown-Forsythe test were performed.

Results

Generation and validation of HeLa Bcl-2 KO cells.

To examine the cell physiological role of Bcl-2, we focused on HeLa cells, in which Bcl-2 is present but not upregulated like in diffuse large B-cell lymphoma (DLBCL) cells. To substantiate this claim, we benchmarked the Bcl-2-protein levels via immunoblotting of lysates of HeLa and of two DLBCL cell lines, SU-DHL-4 and OCI-LY-1, known to have the *BCL2* gene t(14;18) translocation and to be dependent on Bcl-2 for their survival [32]. This immunoblot analysis demonstrated that Bcl-2-protein levels are 10-fold lower in HeLa cells compared to DLBCL cells (Supplemental Figure 1). We then used a CRISPR/Cas9 approach to knockout Bcl-2 in HeLa cells (Bcl-2 KO). Following transfection with a gRNA targeting Bcl-2 while expressing Cas9 (Bcl-2 KO cells), or Cas9 only (control cells), the cells were selected with puromycin for 48h (Fig. 1A), generating Bcl-2 KO and control cell populations. Loss of Bcl-2 expression was validated via immunoblotting (Fig. 1B), indicating that the Bcl-2-protein levels were below the detection limit. The Bcl-2 KO cells displayed normal cell morphology (Supplementary Fig. 2A) and their proliferation was similar to control cells (Supplementary Fig. 2B-C).

Since loss of Bcl-2 could drive potential compensatory effects, we checked the expression levels of two other major anti-apoptotic Bcl-2 family members, Bcl-xL and Mcl-1, via immunoblotting. However, the protein levels of both Bcl-xL and Mcl-1 remained unaltered upon knockout of Bcl-2, indicating that loss of Bcl-2 was not compensated by an upregulation of these anti-apoptotic proteins (Fig. 1C-F). This validates that HeLa cells are not highly dependent on Bcl-2 for their survival under non-stressed conditions.

Furthermore, Bcl-2 KO cells did not display increased caspase-3-mediated poly (ADP-ribose) polymerase (PARP) cleavage compared to control cells (Fig 1G-H). PARP cleavage was quantified via immunoblotting as the percentage of cleaved over total PARP. To further substantiate that HeLa cells are not dependent on Bcl-2 for their survival, we found that in contrast to the DLBCL cell line OCI-LY-1, venetoclax treatment (1 uM, 6 hrs) did not evoke cell death in HeLa cells, as measured by flow cytometry analysis of Annexin V-FITC/7-AAD-stained cells (Supplementary Fig. 3). Collectively, these results firmly validate that loss of Bcl-2 is not critical for HeLa cell survival and proliferation.

To validate that Bcl-2 KO cells display reduced anti-apoptotic reserve, we examined their apoptotic sensitivity to staurosporine (STS), which engages both canonical and IP_3R/Ca^{2+}-dependent signalling pathways [33]. PARP–cleavage was quantified in cells exposed to 0.1 μM STS for 6h. Bcl-2 KO cells displayed an elevation in cleaved PARP levels by 1.2-fold (p=0068) compared to control cells, indicating enhanced sensitivity to STS-induced apoptosis (Fig. 1G-I). Together, these data validate the successful

generation of Bcl-2 KO cells and support their suitability for investigating the non-canonical role of Bcl-2.

Bcl-2 deficiency promotes mitochondrial respiration.

Given Bcl-2's localization at MERCS [13,34] and its redundancy in suppressing basal MOMP, we asked whether non-apoptotic mitochondrial functions such as mitochondrial bioenergetics were affected by loss of Bcl-2. To assess mitochondrial oxidative phosphorylation (OXPHOS), we measured oxygen consumption rates (OCR) in control cells and Bcl-2 KO cells undergoing a "MitoStress" test using Seahorse Analyzer. Overall, Bcl-2 KO cells displayed an increased OCR compared to control cells (Fig. 2A). More specifically, basal respiration, ATP-production coupled respiration, maximal respiration and proton leak were increased in the Bcl-2 KO cells, whereas spare respiratory capacity and non-mitochondrial oxygen consumption remained unchanged (Fig. 2B-G).

Loss of Bcl-2 enhances mitochondrial Ca^{2+} uptake.

Given the high importance of mitochondrial Ca^{2+} levels for driving mitochondrial metabolism, we questioned whether the increase in mitochondrial OXPHOS in Bcl-2 KO cells is accompanied by an increase in ER-mitochondrial calcium transfer. To assess this, we simultaneously monitored the agonist-evoked Ca^{2+} depletion from the ER lumen by using the red ER-targeted Ca^{2+} indicator (R-CEPIA-ER) and the concomitant Ca^{2+} rise in the mitochondrial matrix by using the green mitochondrial matrix-targeted Ca^{2+} indicator (G-CEPIA-3mt). To adequately determine the impact of Bcl-2 on ER-mitochondrial Ca^{2+} transfer, it's important to assess whether the Ca^{2+} release from the ER is similar between control and Bcl-2 KO cells. We previously showed that inhibition of IP_3Rs by Bcl-2 is antagonized by high $[IP_3]$ and thus Bcl-2 fails to inhibit IP_3R-mediated Ca^{2+} release under high $[IP_3]$/[agonist] conditions [35]. Therefore, we compared the agonist-evoked mitochondrial Ca^{2+} rise between control and Bcl-2 KO cells using high [agonist]. Furthermore, by performing the experiments in the presence of extracellular Ca^{2+}-chelating agent EGTA, we further ruled out the contribution of extracellular Ca^{2+} influx into the cell and by extension into the mitochondrial matrix.

We first optimized the agonist concentration to be used for this analysis by performing cytosolic Ca^{2+} measurements in Fura-2-loaded control and Bcl-2 KO HeLa cells exposed to the extracellular agonist ATP. This analysis revealed that 10 µM [ATP] was able to evoke a similar Ca^{2+} rise in the cytosol of control and Bcl-2 KO cells (Fig. 3A-B). Consistently with the cytosolic Ca^{2+} results, 10 µM ATP decreased the ER Ca^{2+} levels to a similar extent in control and Bcl-2 KO cells, further indicating that this concentration of ATP evokes the same level of Ca^{2+} release from the ER, irrespective of Bcl-2 presence (Fig. 3C-D). However, the agonist-evoked mitochondrial Ca^{2+} uptake was significantly elevated by about

1.8-fold (p=0.0156) in Bcl-2 KO cells compared to control cells, indicating a more efficient Ca^{2+} transfer from the ER to the mitochondria in cells lacking Bcl-2 (Fig. 3E-F).

To ensure that this was an on-target of effect of loss of Bcl-2, we assessed the impact of re-expressing Bcl-2 in the Bcl-2 KO cells by transfecting these cells with the 3xFLAG-Bcl-2-P2A-mCherry plasmid. This plasmid produces two proteins, 3xFLAG-Bcl-2 and mCherry, the latter is used to identify transfected and thus Bcl-2-expressing cells. Similar experiments as described above were performed to measure agonist-evoked mitochondrial Ca^{2+} uptake in mCherry-positive cells. These analyses indicated that overexpressed 3xFLAG-Bcl-2 could reverse the elevated mitochondrial Ca^{2+} uptake evoked by 10 µM ATP present in Bcl-2 KO cells, similarly to level of mitochondrial Ca^{2+} uptake observed in control cells (Fig. 4A-B). Additionally, we confirmed that in these conditions, re-expression of 3xFLAG-Bcl-2 in Bcl-2 KO cells did not suppress IP_3R-mediated Ca^{2+} rise in the cytosol by measuring cytosolic Ca^{2+} release in Fura-2-loaded cells (Fig. 4C-D). Taken together, these data indicate that endogenous Bcl-2 suppresses mitochondrial Ca^{2+} influx.

Bcl-2 regulates ER-mitochondrial contact formation to control Ca^{2+} transfer.

Since mitochondrial metabolism and ER-mitochondrial Ca^{2+} transfer are dependent on MERCS, we asked whether the increase in mitochondrial OXPHOS in Bcl-2-KO cells is associated with a change in MERCS. We first checked if loss of Bcl-2 would alter the expression levels of some major ER-mitochondrial tethering proteins, thereby impacting the MERCS. Via immunoblotting, we assessed the protein levels of Mitofusin 2 (Mfn2), GRP75, vesicle-associated membrane protein-associated protein B/C (VAPB), IP_3R (all isoforms) and voltage-dependent anion channel 1 (VDAC1) (Fig. 5 upper panel). Quantification showed that the protein levels of these proteins involved in ER-mitochondrial tethering remained unaltered in Bcl-2 KO cells compared to control cells (Fig. 5 lower panel).

To visualize and quantify MERCS, we used the split GFP-based SPLICS sensors, a validated approach to monitor membrane contact sites [36]. The split-GFP based SPLICS emits green fluorescence when the ER and mitochondria are in close proximity allowing the split GFP to recomplement [37]. Furthermore, SPLICS that specifically sense short contact sites of about 10 nm (visualized through $SPLICS_{short}$), medium contact sites of about 20 nm (visualized through $SPLICS_{medium}$) and long contact sites of about 40 nm (visualized through $SPLICS_{long}$) have been developed. We first quantified short MERCS and found that Bcl-2 KO cells displayed a 47% (p=0.0028) increase in the number of ER-mitochondrial contact sites (Fig. 6A-B). To demonstrate that this effect is due to loss of Bcl-2, we performed a rescue experiment re-expressing Bcl-2 in Bcl-2 KO cells using 3xFLAG-Bcl-2-P2A-mCherry. By analysing the

mCherry-positive cells, 3xFLAG-Bcl-2 decreased the number of ER-mitochondrial contacts to a similar level as observed in control cells (Fig. 6A-B).

Given that ER-mitochondrial Ca^{2+} transfer particularly occurs via MERCS of about 20 nm length [18], we also monitored the impact of loss of Bcl-2 on 20 nm MERCS using $SPLICS_{medium}$. Similarly, to our observations using $SPLICS_{short}$, we found that the number of puncta formed by $SPLICS_{medium}$ too were increased by 70% (p=0.0106) in Bcl-2 KO cells compared to control cells, indicating that not only the number of the 10 nm MERCS but also of 20 nm "Ca^{2+}" MERCS are increased in cells lacking Bcl-2. Also in this case, the increased number of 20 nm MERCS present in Bcl-2 KO cells is suppressed upon re-expression of Bcl-2 (Fig. 6C-D).

As IP_3Rs reside at MERCS, contribute to MERC formation and bind Bcl-2, we questioned whether IP_3Rs could serve as a hub for Bcl-2, enabling its impact on MERCS. For this, we performed Bcl-2 overexpression in wild-type HeLa cells (HeLa WT) and HeLa cells lacking all three isoforms of IP_3Rs (HeLa IP_3R 3KO cells) and transfected with $SPLICS_{medium}$. In line with IP_3Rs' function as tethering proteins at the MERCS, the number of MERCS is decreased by 44% (p=0.0149) in HeLa IP_3R 3KO cells compared to wild-type HeLa cells (Fig. 7). Consistently, overexpression of Bcl-2 decreased the number of MERCS in wild-type HeLa cells to a larger extend compared to HeLa IP_3R 3KO cells. These data indicate that the ability of Bcl-2 to reduce MERCS is, at least partially, dependent on the presence of IP_3Rs.

To further substantiate the regulation of 20 nm MERCS by Bcl-2, we used artificial ER-mitochondrial linkers (EML) to enforce the distance between ER and mitochondria to be 20 nm. We compared the impact of these 20 nm EML on ER-mitochondrial Ca^{2+} transfer in control and Bcl-2 KO HeLa cells. For this, we performed G-CEPIA-3mt-based mitochondrial Ca^{2+} measurements in control and Bcl-2 KO cells exposed to the high [agonist] of 10 µM ATP, either expressing the 20 nm EML or the control plasmid. Extracellular EGTA was used to ensure the mitochondrial Ca^{2+} uptake was only a consequence of the IP_3R-mediated release of Ca^{2+} from the ER stores. Quantification of the AUC of the mitochondrial Ca^{2+} responses revealed that introducing the 20 nm EML in control cells augmented the mitochondrial Ca^{2+} uptake to a similar extent as observed in Bcl-2 KO cells (Fig. 8). Furthermore, introducing the 20 nm EML in Bcl-2 KO cells did not further increase the mitochondrial Ca^{2+} uptake in these cells, indicating that the number of 20 nm MERCS is already nearly maximal in the Bcl-2 KO cells. Taken together, these findings indicate that loss of Bcl-2 augments the number of 20 nm ER-mitochondrial contacts, thereby increasing ER-mitochondrial Ca^{2+} transfer.

Discussion

Bcl-2 is best known for its anti-apoptotic function, protecting cells against pro-apoptotic stress induced by toxic compounds or genomic instability, as observed in cancer. In fact, several types of B-cell malignancies are dependent on elevated Bcl-2 expression to enable cancer cell survival and counteract the upregulation of pro-apoptotic Bcl-2-family members such as BIM [38]. However, the canonical view of Bcl-2 mainly comes from studies performed under stress conditions. Much less is known about the housekeeping function of Bcl-2 in cells that are not exposed to toxic triggers and in which Bcl-2 is not critical for cell survival to oncogenic stress. Addressing this gap is crucial to fully comprehend the broader physiological relevance of Bcl-2.

In this study, we generated a Bcl-2 knockout in HeLa cells, which are not dependent on Bcl-2 for their survival. This has been previously shown by others but was also validated in this work: first, no spontaneous cell death was observed in Bcl-2 KO HeLa cells, and second, HeLa cells did not undergo apoptosis in response to venetoclax, a selective BH3-mimetic Bcl-2 antagonist. Using this cell model, we discovered a novel moonlighting function of Bcl-2 in regulating mitochondrial metabolism beyond its canonical role in apoptosis. More specifically, loss of Bcl-2 enhanced the formation of MERCS, increased ER-mitochondrial Ca^{2+} and eventually promoted mitochondrial metabolism. Re-expression of Bcl-2 in Bcl-2 KO cells reversed these effects, indicating that Bcl-2 acts a negative regulator of ER-mitochondrial coupling.

MERCS allow efficient Ca^{2+} transfer between ER and mitochondria. Because the mitochondrial Ca^{2+} uniporter (MCU) complex is tightly regulated by MICU gatekeeping proteins [39], efficient mitochondrial Ca^{2+} uptake requires locally elevated Ca^{2+} concentrations. These high Ca^{2+} microdomains can be formed when the ER and mitochondrial membranes are brought in close proximity and the spatial distance between these two organelles is crucial in determining the efficiency of the mitochondrial Ca^{2+} uptake. Previous research using molecular linkers to control ER-mitochondrial distance indicated that a distance of 20 nm between the ER and mitochondria is optimal for Ca^{2+} transfer [18]. We found that deletion of Bcl-2 increased the number of ER-mitochondrial contacts within the 20 nm distance but also the shorter contacts within 8-10 nm distance (Fig. 6), indicating that endogenous Bcl-2 limits the number of MERCS. Furthermore, restoring Bcl-2 expression in BCL-2 KO cells reduced the number of contacts, showing an on-target effect of loss of Bcl-2 on MERCS (Fig. 6). This is in line with our previous research, showing that Bcl-2 resides at the MERCs and decreases the number of “short” 10 nm ER-mitochondrial contacts [27]. Additionally, we used a 20 nm ER-mitochondrial linker to set the ER-mitochondrial distance and observed an increase in mitochondrial Ca^{2+} influx in control cells but not in Bcl-2 KO cells (Figure 8). This further supports the

observation that loss of Bcl-2 promotes ER-mitochondrial contact formation at 20 nm distance which facilitates efficient Ca^{2+} transfer towards the mitochondria. Taken together, we hypothesize that Bcl-2 acts as a gatekeeper by reducing the number of ER-mitochondrial contacts within the optimal 20 nm distance range, thereby preventing mitochondrial Ca^{2+} overload. On the other hand, loss of Bcl-2 increases ER-mitochondrial coupling and enhances mitochondrial Ca^{2+} uptake (Fig. 3) and mitochondrial respiration (Fig. 2). Interestingly, besides the observation that MERCS impact Ca^{2+} signalling, it has been shown that Ca^{2+} signals can also, in turn, modulate the formation of MERCS. More specifically, depletion of ER Ca^{2+}-levels enhanced ER-mitochondrial coupling [40].

Moreover, this function of Bcl-2 at the MERCS appears to depend, at least partially, on the presence of IP_3Rs, intracellular Ca^{2+} channels residing at MERCS and contributing to their formation. Consistent with previous reports highlighting the importance of IP_3Rs in maintaining MERCS [41], we found that MERCS are reduced in cells lacking IP_3Rs compared to wild-type cells (Fig. 7). Accordingly, Bcl-2 was less effective in modulating MERCS in cells lacking IP_3Rs, indicating that its regulatory role at the ER-mitochondrial interface is at least partially mediated through IP_3Rs. One possible explanation is that Bcl-2 interferes with the formation or the stability of the IP_3R-GRP75-VDAC1 complex, thereby limiting the tethering between the ER and mitochondria and ultimately limiting efficient mitochondrial Ca^{2+} uptake.

Another important question that is raised is how these non-canonical functions of Bcl-2 relate to its canonical role in apoptosis [42]. The observed increase in ER-mitochondrial coupling in Bcl-2 KO cells could potentially sensitize the mitochondria to apoptotic stimuli facilitating mitochondrial Ca^{2+} overload, a known trigger to MOMP. Thus, in addition to directly inhibiting pro-apoptotic proteins at the mitochondria, Bcl-2 may prevent apoptosis indirectly by limiting Ca^{2+} transfer towards the mitochondria. Future studies are necessary to determine whether these effects of Bcl-2 at the MERCS occur independently from its canonical anti-apoptotic function.

Beyond Bcl-2, other Bcl-2 family members have been identified to play a role at the level of the MERCS and influence Ca^{2+} dynamics. Researchers found that proapoptotic Bcl-2 related ovarian killer (BOK) is located at the MERCS and loss of BOK is capable of reducing the ER-mitochondrial contacts and mitochondrial Ca^{2+} influx [43]. Of note, BOK has been found to tightly bind the IP_3R but loss of BOK caused either no significant changes on cytosolic Ca^{2+} release [44], or reduced cytosolic Ca^{2+} release [45]. On the other hand, overexpression of Mcl-1 was shown to inhibit mitochondrial Ca^{2+} uptake while loss of Mcl-1 increased mitochondrial Ca^{2+} influx [46]. Also Bcl-xL has been found to reside at the MERCS. Overexpression of Bcl-xL showed a decrease in cytosolic Ca^{2+} release while mitochondrial Ca^{2+} influx was increased [47]. However, more recently researchers found that Bcl-xL interacts with VDAC

and thereby reduces mitochondrial Ca^{2+} uptake [48]. Altogether, it is clear that Bcl-2-family members can reside at the MERCS and modulate mitochondrial Ca^{2+} dynamics. However, different Bcl-2-family members may affect Ca^{2+} dynamics through distinct mechanism with potentially different outcomes. Further research will allow to fully understand the non-canonical functions of different Bcl-2-family members at the ER-mitochondrial interface.

The broader relevance of our findings is highlighted by the involvement of Bcl-2 in a number of diseases including cancer and neurodegenerative disorders such as Alzheimer's disease (AD). Beyond its canonical role in apoptosis, Bcl-2 may be particularly relevant in AD through its ability to modulate intracellular Ca^{2+} homeostasis. Increasing evidence indicates dysregulations in Ca^{2+} signalling as an early effect in AD, with excessive ER-Ca^{2+} release through IP_3Rs and RyRs, contributing to mitochondrial Ca^{2+} overload, oxidative stress and neuronal dysfunction [49]. Interestingly, several studies indicate downregulation of Bcl-2 in AD [50,51]. Our results can therefore serve as a mechanistic framework to understand these observations, given that loss or downregulation of Bcl-2 in AD may exacerbate mitochondrial Ca^{2+} overload and metabolic imbalance. On the other hand, protective effects of Bcl-2 overexpression in AD models have been observed [52,53]. These effects might not only arise from inhibition of apoptosis, but also from stabilizing ER-mitochondrial Ca^{2+} coupling.

As mentioned before, cancer cells often rely on Bcl-2 for its survival, as Bcl-2 prevents MOMP by sequestering pro-apoptotic Bcl-2-family members. However, our findings suggest that Bcl-2 can contribute to tumour cell survival though an additional, non-canonical mechanism. By limiting the formation of MERCS and suppressing Ca^{2+} transfer to the mitochondria, Bcl-2 may ultimately prevent mitochondrial Ca^{2+} overload. This mechanism might be particularly relevant in cancer cells that rely heavily on tight control of mitochondrial function to balance the high metabolic demands with survival. Interestingly, through this mechanism, Bcl-2 can contribute to the anti-apoptotic effect in cancer cells independently from its inhibition of pro-apoptotic Bcl-2-family members at the mitochondria.

In conclusion, this study has established endogenous Bcl-2 as a key regulator of ER-mitochondrial dynamics by directly suppressing MERCS and subsequent ER-mitochondrial Ca^{2+} transfer. Our findings identify a novel non-canonical function of Bcl-2 and highlight its broader importance in maintaining cellular homeostasis.

Author contributions

Manon Callens: Conceptualization, Methodology, Investigation, Data curation, Formal analysis, Writing – original draft, funding acquisition. **Jens Loncke**: Conceptualization, Methodology, Investigation, Data curation, Formal analysis, Writing –original draft. **Ophélie Champion**: Conceptualization, Methodology, Investigation, Data curation, Formal analysis, Writing – review and editing. **Dmitry Lim**: Methodology. **Rita La Rovere**: Investigation. **Tim Vervliet**: Conceptualization, Writing – review and editing, Supervision, Funding acquisition. **Geert Bultynck**: Conceptualization, Writing – review and editing, Supervision, Funding acquisition.

Funding

This work was supported by Research Foundation – Flanders [FWO, project numbers G0E7520N (GB), G081821N (GB), G094522N (GB) and fellowships numbers 11K7122N (MC), 12ZG121N (TV), 1230227N (OC)], Research Council – KU Leuven C14/25/131 (GB) and the Central European Leuven Strategic Alliance (CELSA/23/031 and CELSA/23/032). GB is part of the FWO Scientific Research Network CaSign (W0.014.22N).

Acknowledgements

The authors would like to thank Anja Florizoone for the excellent technical assistance. We would like to thank Anthony Letai for OCI-LY-1 and SU-DHL-4 cells and Mikoshiba for HeLa IP_3R 3KO cells. We would also like to thank Feng Zhang for the pSpCas9(BB)-2A-Puro (PX459) plasmid; Masamitsu Iino for the pCMV G-CEPIA-3mt and pCMV R-CEPIA-1ER plamids; Marisa Brini & Tito Calì for SPLICS Mt-ER Short P2A probe (8-10nm, $SPLICS_{short}$).

Generative AI statement

M365 Copilot was used to improve readability of the manuscript. All AI-generated suggestions were critically reviewed and edited by the authors before integration in the manuscript.

Conflict of Interest statement

The authors have no conflict of interests to declare.

Data Availability statement

All data will be made publicly available at the moment of publication via KU Leuven – Research Data Repository (RDR). All raw immunoblots have been uploaded as Supplementary material.

Bibliography

1. Czabotar, P.E.; Garcia-Saez, A.J. Mechanisms of BCL-2 family proteins in mitochondrial apoptosis. *Nat Rev Mol Cell Biol* **2023**, *24*, 732-748, doi:10.1038/s41580-023-00629-4.
2. Green, D.R. The Mitochondrial Pathway of Apoptosis Part II: The BCL-2 Protein Family. *Cold Spring Harb Perspect Biol* **2022**, *14*, doi:10.1101/cshperspect.a041046.
3. Kale, J.; Osterlund, E.J.; Andrews, D.W. BCL-2 family proteins: Changing partners in the dance towards death. *Cell Death and Differentiation* **2018**, *25*, 65-80, doi:10.1038/cdd.2017.186.
4. Qian, S.; Wei, Z.; Yang, W.; Huang, J.; Yang, Y.; Wang, J. The role of BCL-2 family proteins in regulating apoptosis and cancer therapy. *Front Oncol* **2022**, *12*, 985363, doi:10.3389/fonc.2022.985363.
5. Vogler, M.; Braun, Y.; Smith, V.M.; Westhoff, M.A.; Pereira, R.S.; Pieper, N.M.; Anders, M.; Callens, M.; Vervliet, T.; Abbas, M.; et al. The BCL2 family: from apoptosis mechanisms to new advances in targeted therapy. *Signal Transduct Target Ther* **2025**, *10*, 91, doi:10.1038/s41392-025-02176-0.
6. Montero, J.; Letai, A. Why do BCL-2 inhibitors work and where should we use them in the clinic? *Cell Death Differ* **2018**, *25*, 56-64, doi:10.1038/cdd.2017.183.
7. Del Poeta, G.; Postorino, M.; Pupo, L.; Del Principe, M.I.; Dal Bo, M.; Bittolo, T.; Buccisano, F.; Mariotti, B.; Iannella, E.; Maurillo, L.; et al. Venetoclax: Bcl-2 inhibition for the treatment of chronic lymphocytic leukemia. *Drugs Today (Barc)* **2016**, *52*, 249-260, doi:10.1358/dot.2016.52.4.2470954.
8. Leverson, J.D.; Sampath, D.; Souers, A.J.; Rosenberg, S.H.; Fairbrother, W.J.; Amiot, M.; Konopleva, M.; Letai, A. Found in Translation: How Preclinical Research Is Guiding the Clinical Development of the BCL2-Selective Inhibitor Venetoclax. *Cancer Discov* **2017**, *7*, 1376-1393, doi:10.1158/2159-8290.CD-17-0797.
9. Liu, J.; Li, S.; Wang, Q.; Feng, Y.; Xing, H.; Yang, X.; Guo, Y.; Guo, Y.; Sun, H.; Liu, X.; et al. Sonrotoclax overcomes BCL2 G101V mutation-induced venetoclax resistance in preclinical models of hematologic malignancy. *Blood* **2024**, *143*, 1825-1836, doi:10.1182/blood.2023019706.
10. Aufdermauer, J.; de Ridder, I.; Ehsani, M.; Khan, M.; Kale, J.; Frenzel, L.; Andrews, D.; Karamanou, S.; Garcia-Saez, A.J.; Bultynck, G. Cancer-associated BCL-2 mutants reveal mechanisms towards venetoclax resistance. *Advanced Science* **2026**.
11. Vervliet, T.; Parys, J.B.; Bultynck, G. Bcl-2 proteins and calcium signaling: Complexity beneath the surface. *Oncogene* **2016**, *35*, 5079-5092, doi:10.1038/onc.2016.31.
12. Means, R.E.; Katz, S.G. Balancing life and death: BCL-2 family members at diverse ER-mitochondrial contact sites. *FEBS J* **2022**, *289*, 7075-7112, doi:10.1111/febs.16241.
13. Popgeorgiev, N.; Jabbour, L.; Gillet, G. Subcellular Localization and Dynamics of the Bcl-2 Family of Proteins. *Front Cell Dev Biol* **2018**, *6*, 13, doi:10.3389/fcell.2018.00013.
14. Vervliet, T.; Lemmens, I.; Welkenhuyzen, K.; Tavernier, J.; Parys, J.B.; Bultynck, G. Regulation of the ryanodine receptor by anti-apoptotic Bcl-2 is independent of its BH3-domain-binding properties. *Biochem Biophys Res Commun* **2015**, *463*, 174-179, doi:10.1016/j.bbrc.2015.04.131.
15. Monaco, G.; Decrock, E.; Akl, H.; Ponsaerts, R.; Vervliet, T.; Luyten, T.; De Maeyer, M.; Missiaen, L.; Distelhorst, C.W.; De Smedt, H.; et al. Selective regulation of IP3-receptor-mediated Ca2+ signaling and apoptosis by the BH4 domain of Bcl-2 versus Bcl-Xl. *Cell Death Differ* **2012**, *19*, 295-309, doi:10.1038/cdd.2011.97.
16. Ivanova, H.; Vervliet, T.; Monaco, G.; Terry, L.E.; Rosa, N.; Baker, M.R.; Parys, J.B.; Serysheva, I.I.; Yule, D.I.; Bultynck, G. Bcl-2-protein family as modulators of ip3 receptors and other organellar ca2+ channels. *Cold Spring Harbor Perspectives in Biology* **2020**, *12*, a035089, doi:10.1101/cshperspect.a035089.

17. Diokmetzidou, A.; Scorrano, L. Mitochondria-membranous organelle contacts at a glance. *J Cell Sci* **2025**, *138*, doi:10.1242/jcs.263895.
18. Dematteis, G.; Tapella, L.; Casali, C.; Talmon, M.; Tonelli, E.; Reano, S.; Ariotti, A.; Pessolano, E.; Malecka, J.; Chrostek, G.; et al. ER-mitochondria distance is a critical parameter for efficient mitochondrial Ca(2+) uptake and oxidative metabolism. *Commun Biol* **2024**, *7*, 1294, doi:10.1038/s42003-024-06933-9.
19. Szabadkai, G.; Bianchi, K.; Varnai, P.; De Stefani, D.; Wieckowski, M.R.; Cavagna, D.; Nagy, A.I.; Balla, T.; Rizzuto, R. Chaperone-mediated coupling of endoplasmic reticulum and mitochondrial Ca2+ channels. *J Cell Biol* **2006**, *175*, 901-911, doi:10.1083/jcb.200608073.
20. Katona, M.; Bartok, A.; Nichtova, Z.; Csordas, G.; Berezhnaya, E.; Weaver, D.; Ghosh, A.; Varnai, P.; Yule, D.I.; Hajnoczky, G. Capture at the ER-mitochondrial contacts licenses IP(3) receptors to stimulate local Ca(2+) transfer and oxidative metabolism. *Nat Commun* **2022**, *13*, 6779, doi:10.1038/s41467-022-34365-8.
21. Danese, A.; Leo, S.; Rimessi, A.; Wieckowski, M.R.; Fiorica, F.; Giorgi, C.; Pinton, P. Cell death as a result of calcium signaling modulation: A cancer-centric prospective. *Biochim Biophys Acta Mol Cell Res* **2021**, *1868*, 119061, doi:10.1016/j.bbamcr.2021.119061.
22. Murgia, M.; Giorgi, C.; Pinton, P.; Rizzuto, R. Controlling metabolism and cell death: at the heart of mitochondrial calcium signalling. *J Mol Cell Cardiol* **2009**, *46*, 781-788, doi:10.1016/j.yjmcc.2009.03.003.
23. Lalier, L.; Mignard, V.; Joalland, M.P.; Lanoe, D.; Cartron, P.F.; Manon, S.; Vallette, F.M. TOM20-mediated transfer of Bcl2 from ER to MAM and mitochondria upon induction of apoptosis. *Cell Death Dis* **2021**, *12*, 182, doi:10.1038/s41419-021-03471-8.
24. Yu, C.Y.; Yeung, T.K.; Fu, W.K.; Poon, R.Y.C. BCL-XL regulates the timing of mitotic apoptosis independently of BCL2 and MCL1 compensation. *Cell Death Dis* **2024**, *15*, 2, doi:10.1038/s41419-023-06404-9.
25. Rizzuto, R.; Pinton, P.; Carrington, W.; Fay, F.S.; Fogarty, K.E.; Lifshitz, L.M.; Tuft, R.A.; Pozzan, T. Close contacts with the endoplasmic reticulum as determinants of mitochondrial Ca2+ responses. *Science* **1998**, *280*, 1763-1766, doi:10.1126/science.280.5370.1763.
26. Atakpa-Adaji, P.; Ivanova, A. IP(3)R at ER-Mitochondrial Contact Sites: Beyond the IP(3)R-GRP75-VDAC1 Ca(2+) Funnel. *Contact (Thousand Oaks)* **2023**, *6*, 25152564231181020, doi:10.1177/25152564231181020.
27. Loncke, J.; de Ridder, I.; Kale, J.; Wagner, L.; Kaasik, A.; Parys, J.B.; Kerkhofs, M.; Andrews, D.W.; Yule, D.; Vervliet, T.; et al. CISD2 counteracts the inhibition of ER-mitochondrial calcium transfer by anti-apoptotic BCL-2. *Biochim Biophys Acta Mol Cell Res* **2025**, *1872*, 119857, doi:10.1016/j.bbamcr.2024.119857.
28. Bultynck, G.; Szlufcik, K.; Kasri, N.N.; Assefa, Z.; Callewaert, G.; Missiaen, L.; Parys, J.B.; De Smedt, H. Thimerosal stimulates Ca2+ flux through inositol 1,4,5-trisphosphate receptor type 1, but not type 3, via modulation of an isoform-specific Ca2+-dependent intramolecular interaction. *Biochem J* **2004**, *381*, 87-96, doi:10.1042/BJ20040072.
29. Ando, H.; Hirose, M.; Mikoshiba, K. Aberrant IP(3) receptor activities revealed by comprehensive analysis of pathological mutations causing spinocerebellar ataxia 29. *Proc Natl Acad Sci U S A* **2018**, *115*, 12259-12264, doi:10.1073/pnas.1811129115.
30. Vervliet, T.; Duelen, R.; Pradhan, A.; La Rovere, R.; Roderick, H.L.; Sampaolesi, M. Cardiomyocyte differentiation from human induced pluripotent stem cells is delayed following knockout of Bcl-2. *J Cell Sci* **2023**, *136*, doi:10.1242/jcs.260216.
31. Suzuki, J.; Kanemaru, K.; Ishii, K.; Ohkura, M.; Okubo, Y.; Iino, M. Imaging intraorganellar Ca2+ at subcellular resolution using CEPIA. *Nat Commun* **2014**, *5*, 4153, doi:10.1038/ncomms5153.
32. Deng, J.; Carlson, N.; Takeyama, K.; Dal Cin, P.; Shipp, M.; Letai, A. BH3 profiling identifies three distinct classes of apoptotic blocks to predict response to ABT-737 and conventional chemotherapeutic agents. *Cancer Cell* **2007**, *12*, 171-185, doi:10.1016/j.ccr.2007.07.001.

33. Rosa, N.; Ivanova, H.; Wagner, L.E., 2nd; Kale, J.; La Rovere, R.; Welkenhuyzen, K.; Louros, N.; Karamanou, S.; Shabardina, V.; Lemmens, I.; et al. Bcl-xL acts as an inhibitor of IP(3)R channels, thereby antagonizing Ca(2+)-driven apoptosis. *Cell Death Differ* **2022**, *29*, 788-805, doi:10.1038/s41418-021-00894-w.
34. Liu, S.; Pereira, N.A.; Teo, J.J.; Miller, P.; Shah, P.; Song, Z. Mitochondrially targeted Bcl-2 and Bcl-X(L) chimeras elicit different apoptotic responses. *Mol Cells* **2007**, *24*, 378-387.
35. Ivanova, H.; Wagner, L.E., 2nd; Tanimura, A.; Vandermarliere, E.; Luyten, T.; Welkenhuyzen, K.; Alzayady, K.J.; Wang, L.; Hamada, K.; Mikoshiba, K.; et al. Bcl-2 and IP3 compete for the ligand-binding domain of IP3Rs modulating Ca(2+) signaling output. *Cell Mol Life Sci* **2019**, *76*, 3843-3859, doi:10.1007/s00018-019-03091-8.
36. Cali, T.; Bayer, E.M.; Eden, E.R.; Hajnoczky, G.; Kornmann, B.; Lackner, L.; Liou, J.; Reinisch, K.; Rhee, H.W.; Rizzuto, R.; et al. Key challenges and recommendations for defining organelle membrane contact sites. *Nat Rev Mol Cell Biol* **2025**, *26*, 776-796, doi:10.1038/s41580-025-00864-x.
37. Cieri, D.; Vicario, M.; Giacomello, M.; Vallese, F.; Filadi, R.; Wagner, T.; Pozzan, T.; Pizzo, P.; Scorrano, L.; Brini, M.; et al. SPLICS: a split green fluorescent protein-based contact site sensor for narrow and wide heterotypic organelle juxtaposition. *Cell Death Differ* **2018**, *25*, 1131-1145, doi:10.1038/s41418-017-0033-z.
38. Fowler-Shorten, D.J.; Hellmich, C.; Markham, M.; Bowles, K.M.; Rushworth, S.A. BCL-2 inhibition in haematological malignancies: Clinical application and complications. *Blood Rev* **2024**, *65*, 101195, doi:10.1016/j.blre.2024.101195.
39. Marchi, S.; Pinton, P. The mitochondrial calcium uniporter complex: molecular components, structure and physiopathological implications. *J Physiol* **2014**, *592*, 829-839, doi:10.1113/jphysiol.2013.268235.
40. Garcia Casas, P.; Rossini, M.; Pavenius, L.; Saeed, M.; Arnst, N.; Sonda, S.; Fernandes, T.; D'Arsie, I.; Bruzzone, M.; Berno, V.; et al. Simultaneous detection of membrane contact dynamics and associated Ca(2+) signals by reversible chemogenetic reporters. *Nat Commun* **2024**, *15*, 9775, doi:10.1038/s41467-024-52985-0.
41. Bartok, A.; Weaver, D.; Golenar, T.; Nichtova, Z.; Katona, M.; Bansaghi, S.; Alzayady, K.J.; Thomas, V.K.; Ando, H.; Mikoshiba, K.; et al. IP(3) receptor isoforms differently regulate ER-mitochondrial contacts and local calcium transfer. *Nat Commun* **2019**, *10*, 3726, doi:10.1038/s41467-019-11646-3.
42. Morris, J.L.; Gillet, G.; Prudent, J.; Popgeorgiev, N. Bcl-2 Family of Proteins in the Control of Mitochondrial Calcium Signalling: An Old Chap with New Roles. *Int J Mol Sci* **2021**, *22*, doi:10.3390/ijms22073730.
43. Carpio, M.A.; Means, R.E.; Brill, A.L.; Sainz, A.; Ehrlich, B.E.; Katz, S.G. BOK controls apoptosis by Ca(2+) transfer through ER-mitochondrial contact sites. *Cell Rep* **2021**, *34*, 108827, doi:10.1016/j.celrep.2021.108827.
44. Schulman, J.J.; Wright, F.A.; Kaufmann, T.; Wojcikiewicz, R.J.H. The Bcl-2 protein family member Bok binds to the coupling domain of inositol 1,4,5-trisphosphate receptors and protects them from proteolytic cleavage. *J Biol Chem* **2013**, *288*, 25340-25349, doi:10.1074/jbc.M113.496570.
45. D'Orsi, B.; Engel, T.; Pfeiffer, S.; Nandi, S.; Kaufmann, T.; Henshall, D.C.; Prehn, J.H. Bok Is Not Pro-Apoptotic But Suppresses Poly ADP-Ribose Polymerase-Dependent Cell Death Pathways and Protects against Excitotoxic and Seizure-Induced Neuronal Injury. *J Neurosci* **2016**, *36*, 4564-4578, doi:10.1523/JNEUROSCI.3780-15.2016.
46. Minagawa, N.; Kruglov, E.A.; Dranoff, J.A.; Robert, M.E.; Gores, G.J.; Nathanson, M.H. The anti-apoptotic protein Mcl-1 inhibits mitochondrial Ca2+ signals. *J Biol Chem* **2005**, *280*, 33637-33644, doi:10.1074/jbc.M503210200.
47. Williams, A.; Hayashi, T.; Wolozny, D.; Yin, B.; Su, T.C.; Betenbaugh, M.J.; Su, T.P. The non-apoptotic action of Bcl-xL: regulating Ca(2+) signaling and bioenergetics at the ER-

mitochondrion interface. *J Bioenerg Biomembr* **2016**, *48*, 211-225, doi:10.1007/s10863-016-9664-x.

48. Andrea Puebla-Huerta, P.M.-C., Camila Quezada- Gutierez, César Casanova-Canelo, Roberto Rosales-Rojas, José Alberto López-Domínguez, Inés Marin, Sandra A. Niño, Pablo Cruz, Micheel Saldivia-Piña, Sergio Linsambarth, Osman Díaz- Rivera, Oscar Cerda, Ariela Vergara-Jaque, Manuel Serrano, Christian Gonzalez-Billault, Ulises Ahumada-Castro, J. César Cárdenas. Bcl-xL interaction with VDAC1 reduces mitochondrial Ca2+ uptake, allowing the establishment of Therapy-Induced Senescence. **2025**.
49. Mustaly-Kalimi, S.; Gallegos, W.; Steinbrenner, D.; Gupta, S.; Houcek, A.J.; Bennett, D.A.; Marr, R.A.; Peterson, D.A.; Sekler, I.; Stutzmann, G.E. Mitochondrial dysfunction mediated by ER-calcium dysregulation in neurons derived from Alzheimer's disease patients. *Acta Neuropathol Commun* **2025**, *13*, 165, doi:10.1186/s40478-025-02023-x.
50. Callens, M.; Kraskovskaya, N.; Derevtsova, K.; Annaert, W.; Bultynck, G.; Bezprozvanny, I.; Vervliet, T. The role of Bcl-2 proteins in modulating neuronal Ca(2+) signaling in health and in Alzheimer's disease. *Biochim Biophys Acta Mol Cell Res* **2021**, *1868*, 118997, doi:10.1016/j.bbamcr.2021.118997.
51. Paradis, E.; Douillard, H.; Koutroumanis, M.; Goodyer, C.; LeBlanc, A. Amyloid β peptide of Alzheimer's disease downregulates bcl-2 and upregulates bax expression in human neurons. *Journal of Neuroscience* **1996**, *16*, 7533-7539, doi:10.1523/jneurosci.16-23-07533.1996.
52. Rohn, T.T.; Vyas, V.; Hernandez-Estrada, T.; Nichol, K.E.; Christie, L.A.; Head, E. Lack of pathology in a triple transgenic mouse model of Alzheimer's disease after overexpression of the anti-apoptotic protein Bcl-2. *Journal of Neuroscience* **2008**, *28*, 3051-3059, doi:10.1523/JNEUROSCI.5620-07.2008.
53. Chernyuk, D.; Callens, M.; Polozova, M.; Gordeev, A.; Chigriai, M.; Rakovskaya, A.; Ilina, A.; Pchitskaya, E.; Van den Haute, C.; Vervliet, T.; et al. Neuroprotective properties of anti-apoptotic BCL-2 proteins in 5xFAD mouse model of Alzheimer's disease. *IBRO Neurosci Rep* **2023**, *14*, 273-283, doi:10.1016/j.ibneur.2023.02.005.

Figure Legends

Fig. 1 Generation and validation of HeLa Bcl-2 KO cells. **A** Schematic overview of the generation of HeLa Bcl-2 KO cells **B** Representative immunoblot of Bcl-2 protein expression levels in control cells and Bcl-2 KO cells (n=9). **C** Immunoblot of control cells and Bcl-2 KO cells stained for Bcl-xL. **D** Densitometric quantification of Bcl-xL protein levels, relative to loading control (*n=8)*. Statistically significant differences were determined with Wilcoxon test. Differences were considered significant when $p < 0.05$. **E** Immunoblot of control cells and Bcl-2 KO cells stained for Mcl-1. **F** Densitometric quantification of Mcl-1 protein levels relative to loading control (*n=8*). Statistically significant differences were determined with paired Student's t-test. Differences were considered significant when $p < 0.05$. **G** Immunoblot of control cells and Bcl-2 KO cells treated with either DMSO or 0.1 µM staurosporine (STS) for 6h, stained for PARP. $PARP_U$: uncleaved PARP; $PARP_C$: cleaved PARP. **H** Densitometric quantification of the % of PARP cleaved (Cleaved PARP/total PARP *100) in control cells and Bcl-2 KO cells treated with DMSO for 6h (*n=5*). Statistically significant differences were determined with paired Student's t-test. Differences were considered significant when $p < 0.05$. **I** Densitometric quantification of the % of PARP cleaved (Cleaved PARP/total PARP *100) in control cells and Bcl-2 KO cells treated with 0.1 µM STS for 6h (*n=6*). Statistically significant differences were determined with paired Student's t-test. Differences were considered significant when $p < 0.05$.

Fig. 2 Loss of Bcl-2 enhances mitochondrial respiration. **A** Average traces of oxygen consumption rate measured in HeLa Bcl-2 KO cells and control cells. Quantification of **B** basal respiration, **C** ATP-production coupled respiration, **D** proton leak, **E** maximal respiration, **F** spare respiratory capacity and **G** non-mitochondrial oxygen consumption. Data are represented as the average ± S.D (*n=5*). Different symbol shapes correspond to different dates of acquisition. Statistically significant differences were determined with paired Student's t-test. Differences were considered significant when $p < 0.05$

Fig. 3 Loss of Bcl-2 promotes mitochondrial Ca^{2+} uptake. **A** Example traces of HeLa Bcl-2 KO and control cells loaded with Fura-2-AM and treated with 10 µM ATP to elicit an IP_3R-mediated response. Extracellular Ca^{2+} was chelated using 3 mM EGTA. **B** Quantification of the area under the curve (AUC) of the ATP response. Data are represented as the average ± S.D (*n=12*). Different symbol shapes correspond to different dates of acquisition. Data is normalized to control. Statistically significant differences were determined with a Student's t-test. Differences were considered significant when $p < 0.05$. **C** Example traces of ER Ca^{2+} efflux measured in HeLa Bcl-2 KO and control cells transfected with R-CEPIA-ER, after chelation of extracellular Ca^{2+} with 3 mM EGTA and agonist stimulation with 10 µM ATP. **D** Quantification of the area under the curve (AUC) of ER Ca^{2+} efflux. Data are represented as the average ± S.D (*n=10-11*). Different symbol shapes correspond to different dates of acquisition. Data is normalized to control. Statistically significant differences were determined with a Welch's t-test. Differences were considered significant when $p < 0.05$. **E** Example traces of mitochondrial Ca^{2+} influx

measured in HeLa Bcl-2 KO and control cells transfected with G-CEPIA-3mt, after chelation of extracellular Ca^{2+} with 3 mM EGTA and agonist stimulation with 10 µM ATP. **F** Quantification of the area under the curve (AUC) of the mitochondrial Ca^{2+} influx. Data are represented as the average ± S.D (*n=10-11*). Different symbol shapes correspond to different dates of acquisition. Data is normalized to control. Statistically significant differences were determined with a Student's t-test. Differences were considered significant when $p < 0.05$.

Fig. 4 Restoring Bcl-2 expression in Bcl-2 KO cells reverses the increased ER-mitochondrial Ca^{2+} transfer. **A** Example traces of HeLa Bcl-2 KO and control cells transfected with Bcl-2 or control in combination withG-CEPIA-3mt. Extracellular Ca^{2+} was chelated using 3 mM EGTA and 10 µM ATP was used to elicit an IP_3R-mediated Ca^{2+} response. **B** Quantification of the area under the curve (AUC) of the mitochondrial Ca^{2+} influx. Data are represented as the average ± S.D (*n=19-22*). Different symbol shapes correspond to different dates of acquisition. Data is normalized to control. Statistically significant differences were determined with a Kruskal-Wallis test. Differences were considered significant when $p < 0.05$. **C** Example traces of HeLa Bcl-2 KO and control cells transfected with Bcl-2 or control and loaded with Fura-2-AM, and treated with 1 µM ATP to elicit an IP_3R-mediated response. Extracellular Ca^{2+} was chelated using 3 mM EGTA. **D** Quantification of the area under the curve (AUC) of the ATP response. Data are represented as the average ± S.D (*n=13-14*). Different symbol shapes correspond to different dates of acquisition. Data is normalized to control. Statistically significant differences were determined with a one-way ANOVA. Differences were considered significant when $p < 0.05$

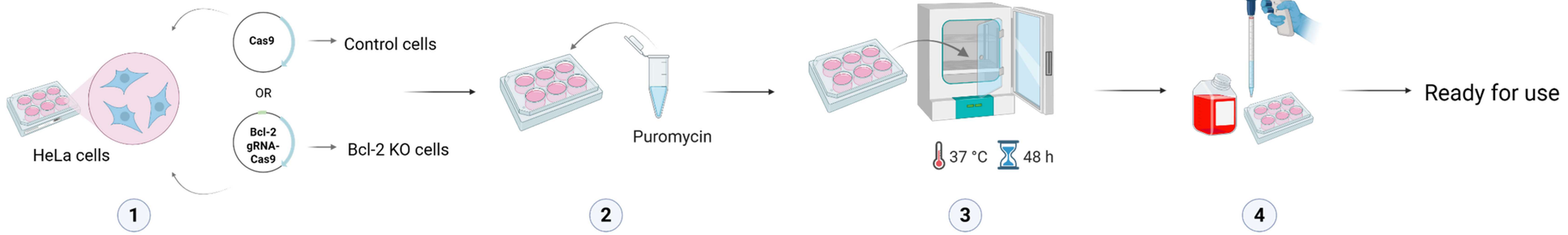
Fig. 5 Loss of Bcl-2 does not affect expression levels of ER-mitochondrial tethering proteins. Representative immunoblot (upper panel) and densitometric quantification relative to loading control (lower panel) of **A** Mitofusin 2 (Mfn2) (*n=7*), **B** IP3R (*n=5*), **C** GRP75 (*n=6*), **D** voltage-dependent anion channel 1 (VDAC1) (*n=5*) and **E** vesicle-associated membrane protein-associated protein B/C (VAPB) (*n=5*). Statistically significant differences were determined with paired Student's t-test. Differences were considered significant when $p < 0.05$.

Fig. 6 Bcl-2 regulates the formation of ER-mitochondrial contacts. **A** Example images of Bcl-2 KO and control cells transfected with $SPLICS_{short}$ and either pCMV24 -P2A-mcherry or pCMV24-Bcl-2-P2A-mcherry. Scale bar indicates 20 µm. **B** Quantification of the number of $SPLICS_{short}$ contacts. Data are represented as the average ± S.D (*n=5*). Different symbol shapes correspond to different dates of transfection. Statistically significant differences were determined with one-way ANOVA. Differences were considered significant when $p < 0.05$. **C** Example images of Bcl-2 KO and control cells transfected with $SPLICS_{medium}$ and either pCMV24-control-P2A-mcherry or pCMV24-Bcl-2-P2A-mcherry. Scale bar indicates 20 µm. **D** Quantification of the number of $SPLICS_{medium}$ contacts. Data are represented as the average ± S.D (*n=5*). Different symbol shapes correspond to different dates of acquisition. Statistically significant differences were determined with one-way ANOVA. Differences were considered significant when $p < 0.05$

Fig. 7 The effect of Bcl-2 at the MERCS is, at least partially, dependent on the presence of IP_3Rs. **A** Example images of wild-type HeLa (WT) and HeLa cells lacking all three isoforms of IP_3Rs (3KO) transfected with $SPLICS_{medium}$ and either pCMV24 -P2A-mcherry (EV) or pCMV24-Bcl-2-P2A-mcherry (Bcl-2). Scale bar indicates 20 µm. **B** Quantification of the number of $SPLICS_{medium}$ contacts. Data are represented as the average ± S.D (n=6-8). Different symbol shapes correspond to different coverslips. Statistically significant differences were determined with two-way ANOVA. Differences were considered significant when $p < 0.05$.

Fig. 8 Fixing ER-mitochondrial distance at 20 nm enhances the level of ER-mitochondrial Ca^{2+} transfer in control cells to the level in Bcl-2 KO cells. **A** Example traces of HeLa Bcl-2 KO and control cells transfected with 20 nm-EML or control and G-CEPIA-3mt. Extracellular Ca^{2+} was chelated with 3 mM EGTA and agonist stimulation of 10 µM ATP was used. **B** Quantification of the area under the curve (AUC) of the mitochondrial Ca^{2+} influx. Data are represented as the average ± S.D (*n=12-14*). Different symbol shapes correspond to different dates of acquisition. Data is normalized to control. Statistically significant differences were determined with Kruskal-Wallis test. Differences were considered significant when $p < 0.05$

A



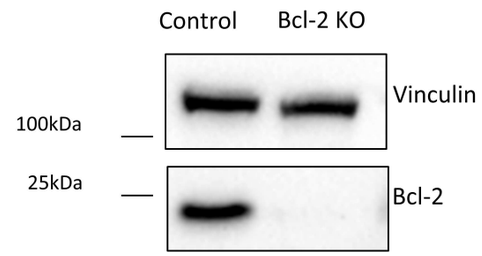
Transfect HeLa cells with Bcl-2 gRNA with Cas9 or with Cas9 only

Perform selection by adding 2µg/mL puromycin

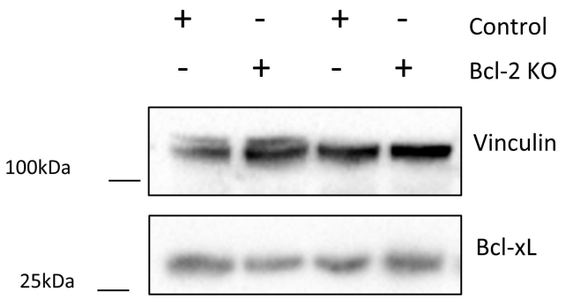
Incubate cells for 48h

Change medium and incubate cells until 80% confluency

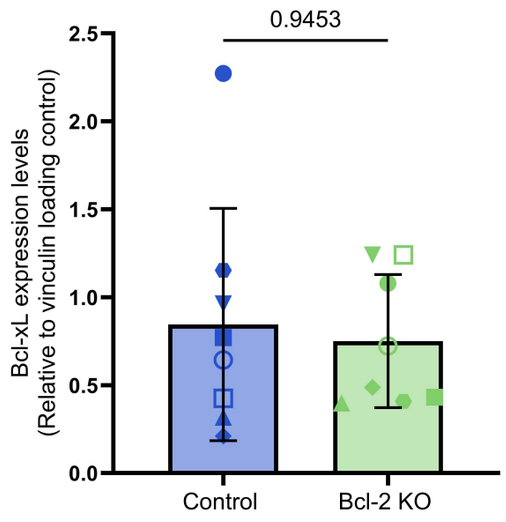
B



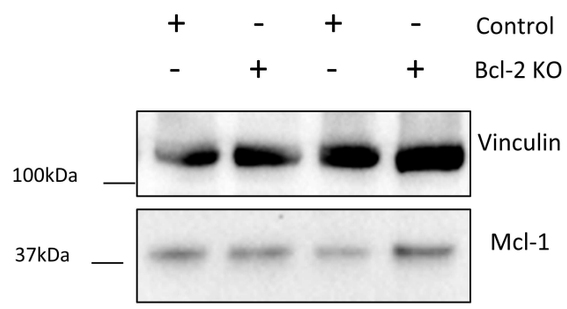
C



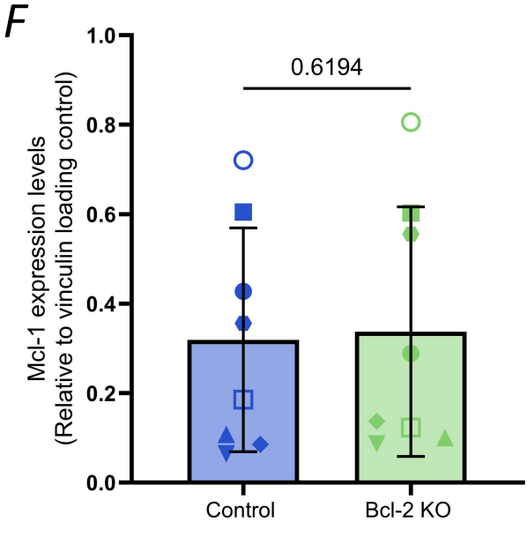
D



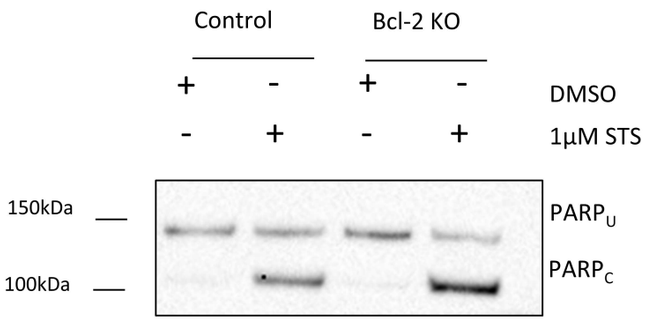
E



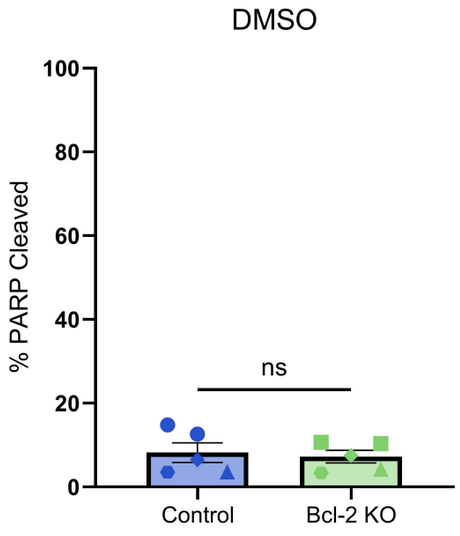
F



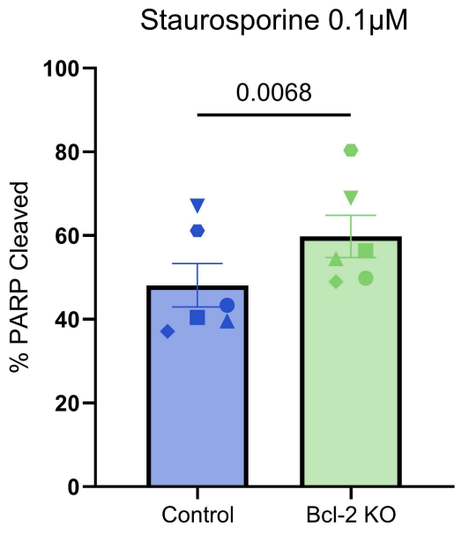
G

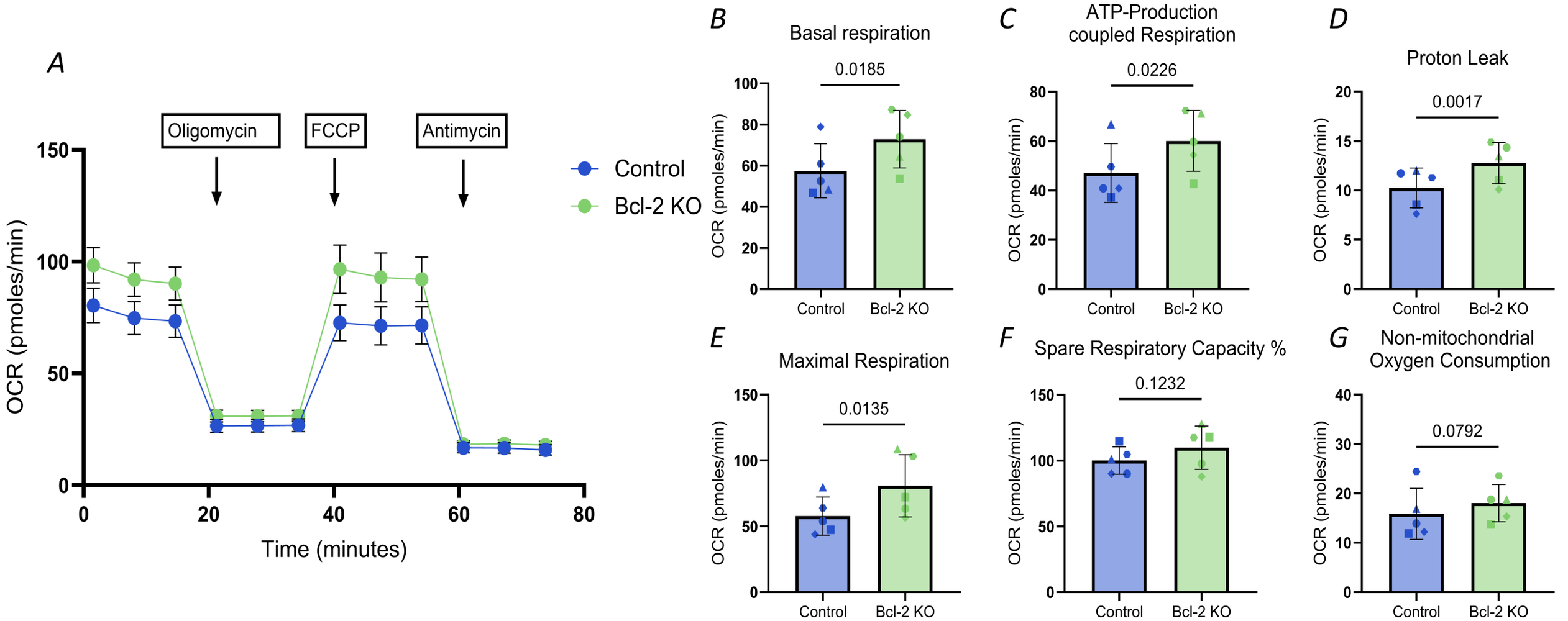


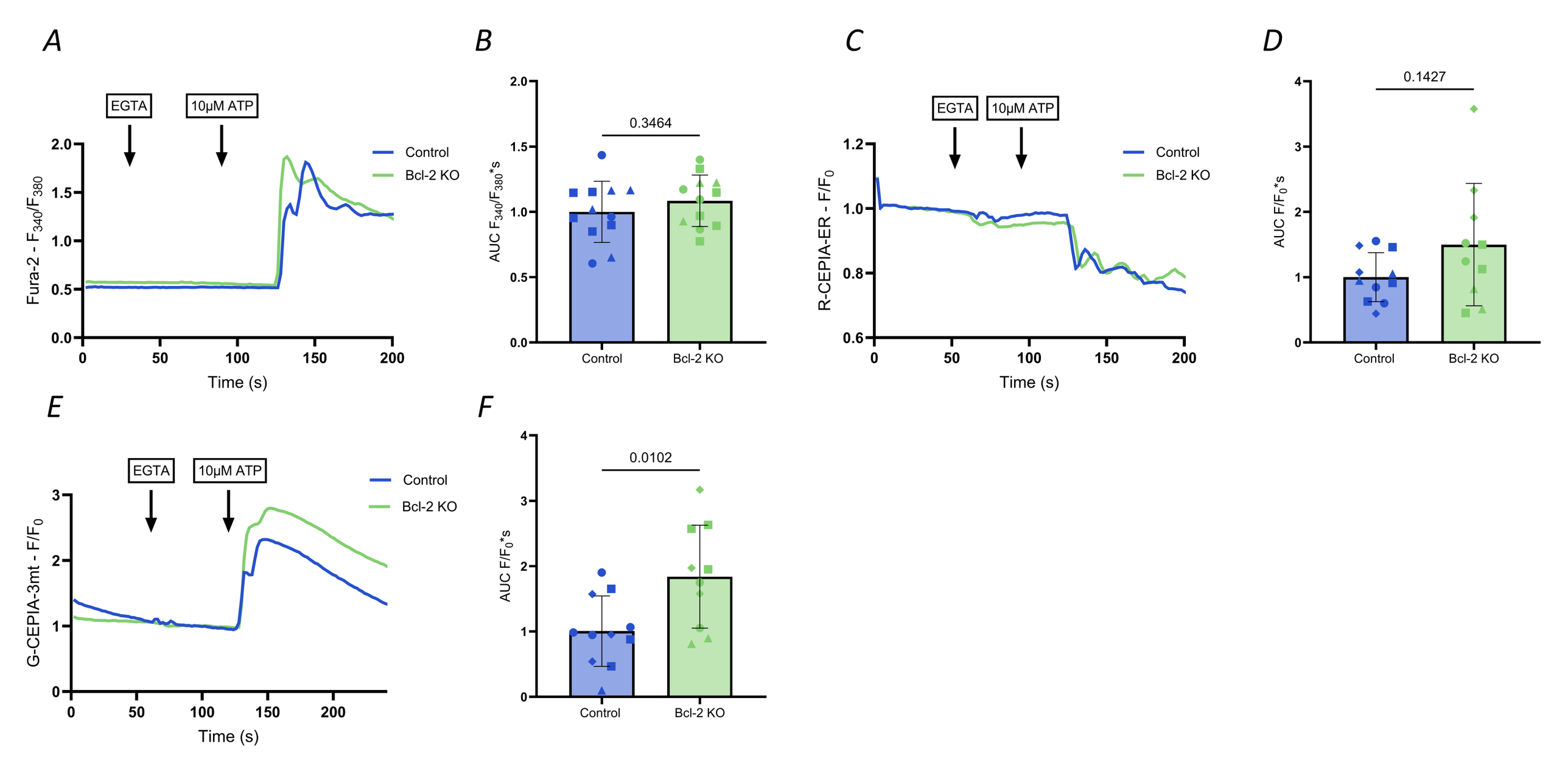
H

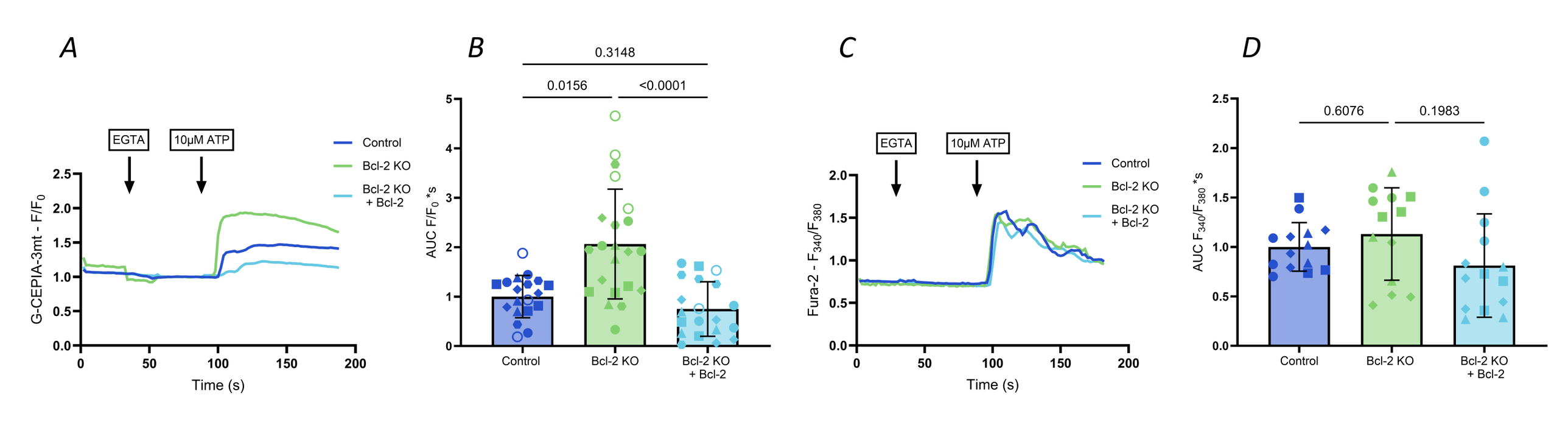


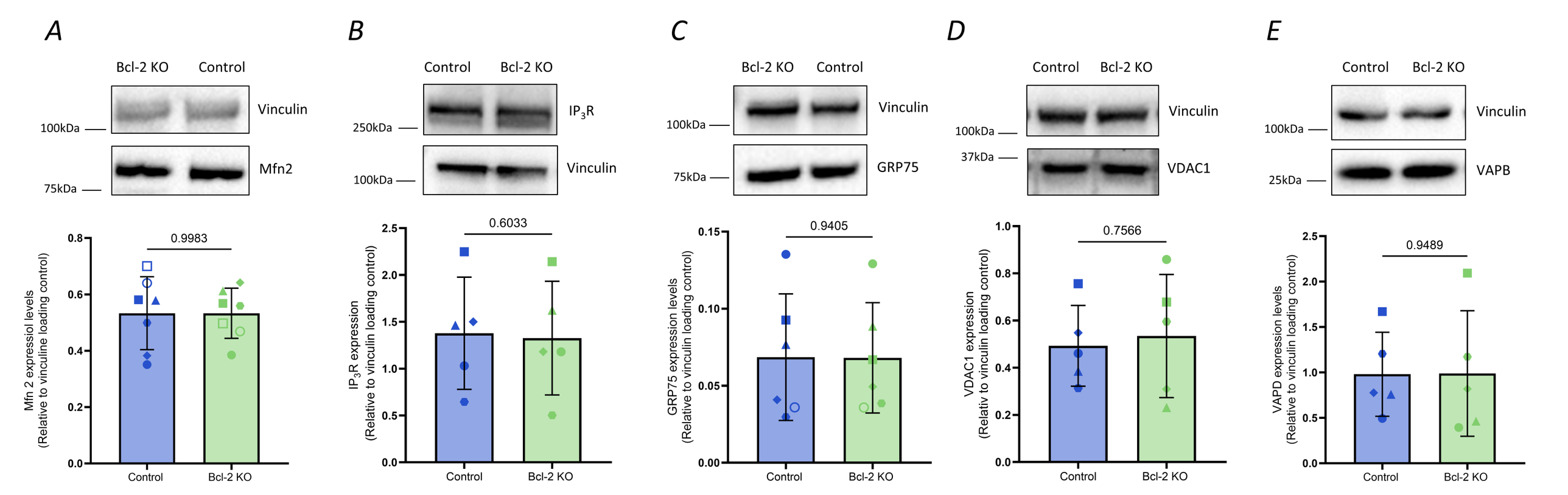
I

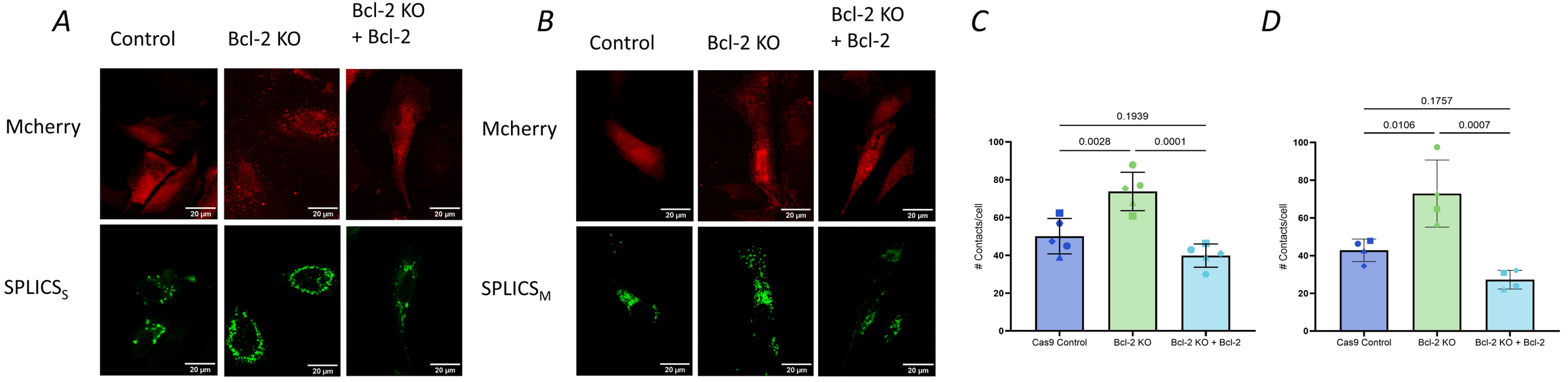


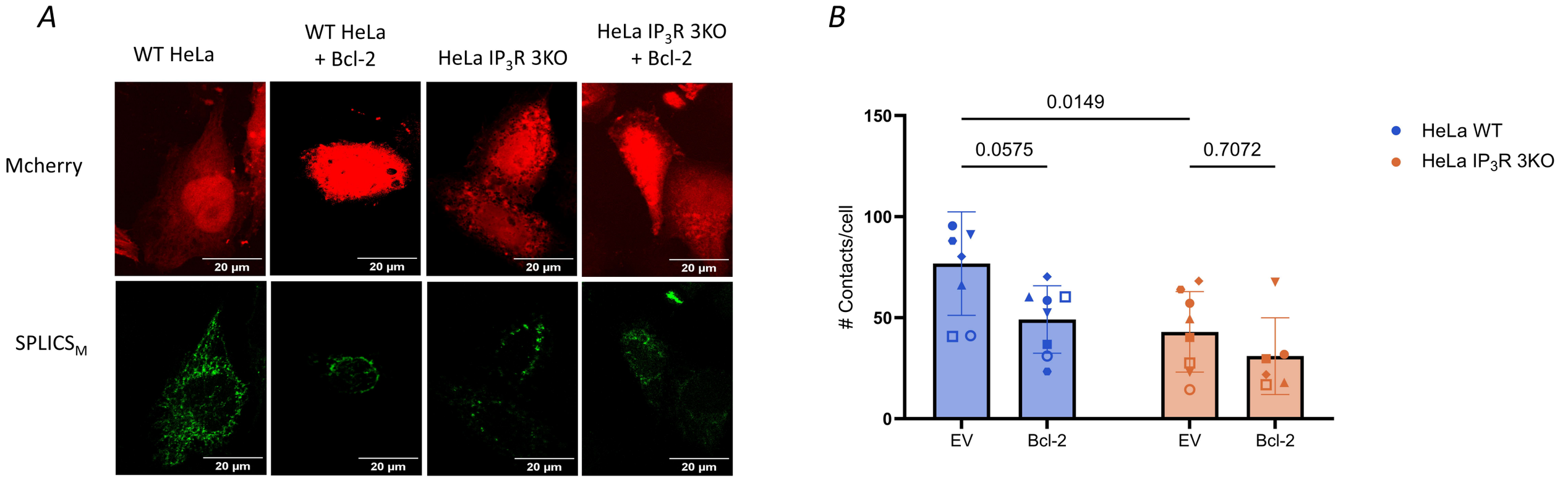

A
Oligomycin
FCCP
Antimycin
Control
Bcl-2 KO
OCR (pmoles/min)
Time (minutes)
B
Basal respiration
0.0185
C
ATP-Production coupled Respiration
0.0226
D
Proton Leak
0.0017
E
Maximal Respiration
0.0135
F
Spare Respiratory Capacity %
0.1232
G
Non-mitochondrial Oxygen Consumption
0.0792

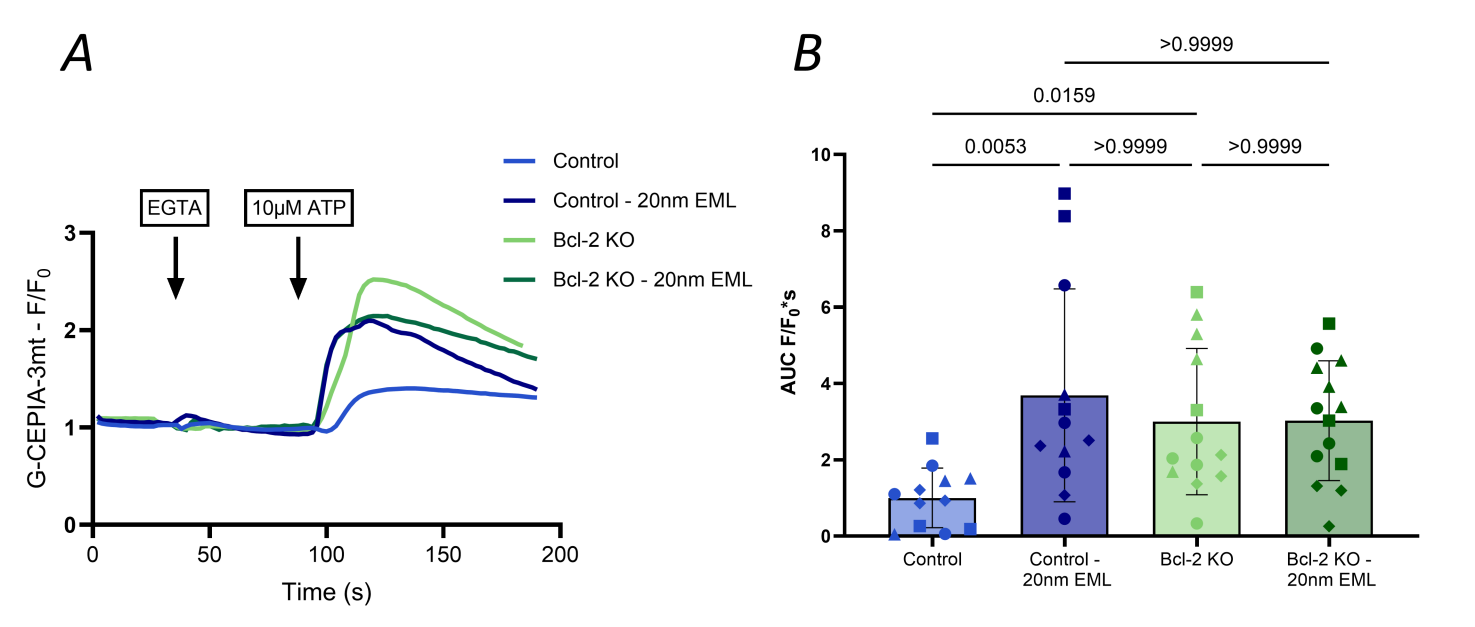

A
EGTA
10μM ATP
Control
Bcl-2 KO
Fura-2 - F340/F380
Time (s)
B
0.3464
AUC F340/F380*s
Control
Bcl-2 KO
C
EGTA
10μM ATP
Control
Bcl-2 KO
R-CEPIA-ER - F/F0
Time (s)
D
0.1427
AUC F/F0*s
Control
Bcl-2 KO
E
EGTA
10μM ATP
Control
Bcl-2 KO
G-CEPIA-3mt - F/F0
Time (s)
F
0.0102
AUC F/F0*s
Control
Bcl-2 KO


A
EGTA
10μM ATP
Control
Bcl-2 KO
Bcl-2 KO + Bcl-2
G-CEPIA-3mt - F/F0
Time (s)
B
0.3148
0.0156
<0.0001
AUC F/F0 *s
Control
Bcl-2 KO
Bcl-2 KO + Bcl-2
C
EGTA
10μM ATP
Control
Bcl-2 KO
Bcl-2 KO + Bcl-2
Fura-2 - F340/F380
Time (s)
D
0.6076
0.1983
AUC F340/F380 *s
Control
Bcl-2 KO
Bcl-2 KO + Bcl-2


A
Bcl-2 KO
Control
100kDa
Vinculin
75kDa
Mfn2
Mfn 2 expressiol levels
(Relative to vinculine loading control)
0.9983
Control
Bcl-2 KO
B
Control
Bcl-2 KO
250kDa
IP3R
100kDa
Vinculin
IP3R expression
(Relative to vinculin loading control)
0.6033
Control
Bcl-2 KO
C
Bcl-2 KO
Control
100kDa
Vinculin
75kDa
GRP75
GRP75 expression levels
(Relative to vinculin loading control)
0.9405
Control
Bcl-2 KO
D
Control
Bcl-2 KO
100kDa
Vinculin
37kDa
VDAC1
VDAC1 expression
(Relativ to vinculin loading control)
0.7566
Control
Bcl-2 KO
E
Control
Bcl-2 KO
100kDa
Vinculin
25kDa
VAPB
VAPD expression levels
(Relative to vinculin loading control)
0.9489
Control
Bcl-2 KO


A
Control
Bcl-2 KO
Bcl-2 KO + Bcl-2
Mcherry
SPLICS$_S$
20 µm
B
Control
Bcl-2 KO
Bcl-2 KO + Bcl-2
Mcherry
SPLICS$_M$
20 µm
C
0.1939
0.0028
0.0001
Contacts/cell
100
80
60
40
20
0
Cas9 Control
Bcl-2 KO
Bcl-2 KO + Bcl-2
D
0.1757
0.0106
0.0007
Contacts/cell
100
80
60
40
20
0
Cas9 Control
Bcl-2 KO
Bcl-2 KO + Bcl-2


A
WT HeLa
WT HeLa + Bcl-2
HeLa IP3R 3KO
HeLa IP3R 3KO + Bcl-2
Mcherry
SPLICSM
20 µm
B
0.0149
0.0575
0.7072
150
100
50
0
Contacts/cell
EV
Bcl-2
EV
Bcl-2
HeLa WT
HeLa IP3R 3KO


A
B
Control
Control - 20nm EML
Bcl-2 KO
Bcl-2 KO - 20nm EML
EGTA
10μM ATP
G-CEPIA-3mt - F/F0
Time (s)
AUC F/F0*s
0.0159
>0.9999
0.0053
>0.9999
>0.9999
Control
Control - 20nm EML
Bcl-2 KO
Bcl-2 KO - 20nm EML

Supplementary Files

This is a list of supplementary files associated with this preprint. Click to download.

- Originalwesternblots.pdf
- Supplementaryfigures.pdf